Current Flow Mechanisms and Photoelectric Properties of Solar Cells Based on p-CdTe-n-CdS and p-CdTe-n-CdSe Heterostructures with Deep Impurity Levels

Salim Otajonov[1*], *Ravshanbek* Ergashev[1] *and Qodir* Botirov[1]

[1] Fergana State University, 150100, Fergana City, Uzbekistan

Abstract. In this paper, we consider the mechanisms of the flow current and photoelectric properties of solar cells manufactured on the basis of strongly mismatched semiconductor p-CdTe-n-CdS and p-CdTe-n-CdSe heterojunctions with a low density of surface states $N=3\cdot10^{11}sm^{-2}$. It was found that the forward current in heterojunctions is due to tunneling of thermally excited electrons, and at large forward biased currents, thermionic nature. The reverse current of such structures has a tunneling nature. It is shown that the structures have a photoconversion efficiency of 0.7 and 0.8 el/sq in the spectral region of 0.4 and 3.0 eV in the near-infrared region of the spectrum.

1 Introduction

CdTe has attracted more attention these days due to its growing use in products such as semiconductor devices, photovoltaics, optoelectronics, laser materials, infrared photodetectors, solar energy converters. Cadmium telluride, being a promising material for solar cells and infrared photodetectors [1, 2]. CdTe is a compound semiconductor and is usually crystallized in hexagonal and cubic structure. High absorption coefficient and almost ideal direct band gap, which is in the center of the solar spectrum [3]. When it comes to practical application in large scale photovoltaics, solar cells using CdTe, which stand out with an efficiency of 16.5% [4].

The solar cell based on cadmium telluride has the maximum photocurrent achieved with a typical global spectrum normalized to 100 mWt/cm^2. Due to the influence of size and different nanostructures, nanoparticles have better mechanical, electrical and optical properties [5]. Deposition [6], pulsed laser technology [7], thermal evaporation [8] and other methods are used to obtain CdTe. Due to its various advantages, thermal evaporation with the addition of impurity elements gives higher performance, which is both interesting and potentially useful. Defects and impurities introduced during the deposition process can positively affect the optical and electrophysical properties to improve the efficiency of solar cells by changing the photovoltaic characteristics of thin films.

* Corresponding author: otajonov_s@mail.ru

In this regard, the coupling of CdTe with cadmium sulfide was investigated, since it increases the efficiency of photosensitivity, due to the charge carriers from CdS to CdTe and also the transition of the generation of charge carriers from deep impurity levels, which increases a significant increase in photosensitivity.

In such heterostructures the influence of surface recombination is significantly reduced due to the influence of impurity levels [9]. The authors of these works [10] by the method of transient processes of contact photoconductivity in CdTe films determined the rate of surface recombination, which is equal to $\tau_R \approx 19$ ns. In these works also determined the dominant deep level with photoionization energies of 1.23 eV, which lead to a decrease in the effect of surface recombination. Since due to high surface recombination these structures for practical purposes are little used for the manufacture of devices, such as high-speed photodetectors. In order to reduce surface recombination, ligations of various elements of group I were used to compensate for their electrical conductivity [11].

In this paper, we describe Ag-doped CdTe heterostructures by thermal evaporation and investigate their current flow mechanisms and photovoltaic properties of solar cells based on p-CdTe-nCdS and pCdTe-nCdSe heterostructures with deep impurity levels.

2 Methodology

Obtaining CdS-CdTe heterostructure of good quality by conventional technological methods in high vacuum, although their different crystal structure (hexagonal and cubic for CdS and CdTe, respectively), as well as a large mismatch of lattice constants (~10%) and thermal expansion coefficients ($\sim 10^{-6}$ K^{-1}) [12]. The combined effect of these factors leads to a large density of surface states N, at the interface, which sharply deteriorate the characteristics of the HS and this can be eliminated with the help of optimal production technology. The value of N, in CdTe-CdS structures can be significantly reduced by the use of group I dopants [13].

The samples were obtained by isothermal annealing in Te vapor of single-crystalline CdS substrates with electron concentration about 10^{18} sm^{-3} at 300°C. Annealing was carried out at 250-300°C for 0.5 to 1.5 h.

The prepared substrates were placed in a special holder and a silver impurity was deposited on the surface of the glass and molybdenum substrate at a temperature of 250°-300°C in a vacuum of about 10^{-5} mm Hg from a separate crucible. The mass of the alloying agent was usually 0.3-0.1 wt % of the mass of the main semiconductor compound, which was evaporated from another crucible. A thin layer of impurity with an effective thickness of 0.1 nm was deposited on the surface, an island layer of material was formed, which subsequently diffused into the layer of the deposited semiconductor film. The exact amount of the introduced impurity was impossible to establish due to the complexity of the metal deposition process on the substrate, and the time t, thickness d and vk (the CdTe deposition rate) were determined experimentally to obtain the best photosensitive heterostructure: t≈15-20 min., v_k to 1.5 nm/s, d≤1 μm. The CdTe condensation rate, determined from the ratio of film thickness to deposition time, was 0.2–2.5 nm/s.

3 Experimental results and their discussion

As a result of processing, a layer of hole conduction is formed on the surface of the initial crystal, the thickness of which is determined by temperature and annealing time. The study of optical transmittance and photosensitivity spectra indicates the formation of a varison structure CdS_x Te_{1-x}, limited on the surface side by a layer of p-CdTe, and on the crystal volume side by n-CdS [14]. The concentrations of which are equal to $n=10^{17}$ sm^{-3}.

The structures exhibited pronounced diode characteristics with a rectification ratio of at least 10^4 at 300 K and voltage U =1 V.

The transition thickness d_0 at zero bias, found from capacitive measurements, depends on the temperature and duration of annealing and is in the range of 0.3 to 2 μm. The value of d_0 relatively weakly affects the spectral distribution of photosensitivity, but significantly determines the mechanism of current flow, as well as the absolute values of photocurrent and photoemfs. In this connection, the studied structures were conditionally divided into three types: A (d_0=0.3 to 0.5), B (d_0=0.5 to 0.1), and C ($d_0 \gtrsim 0.1$ mkm).

The volt-faradic characteristics (VFC) have a different appearance depending on the type of HS. The capacitance C of structures with $d_0 \gtrsim 1$ μm is weakly dependent on voltage. At the same time, for diodes of types A and B, the dependence of C^{-2} on V is linear (Fig. 1), which is characteristic of transitions with sharp impurity distribution. The measurements show that the hole concentration is $p_0 \lesssim 10^{16}$ см$^{-3}$, which is significantly smaller than the electron concentration in the original CdS crystals ($n_0 \simeq 10^{18}$ см$^{-3}$). Hence, the bulk charge is located in CdTe and the solid solution layer $CdS_x Te_{1-x}$.

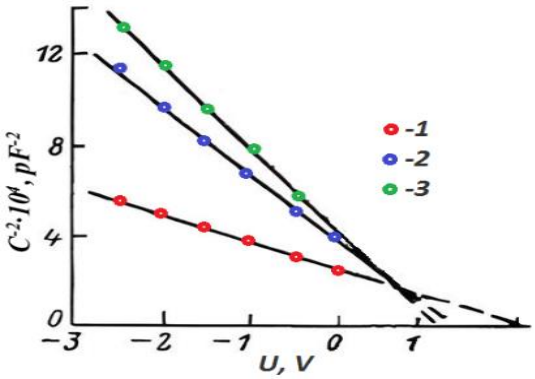

Fig. 1. Volt-farad characteristic of B-type heterojunction at different frequencies. f, MHz: 1 - 0.1, 2 - 0.5, 3 - 1.0.

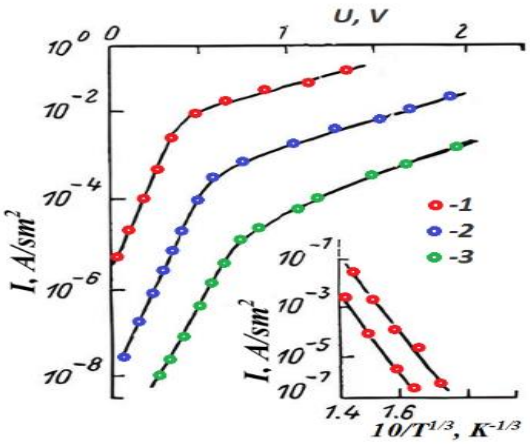

Fig. 2. Straight branches of volt-ampere characteristic of heterojunction type A at different temperatures. T, K: 1 - 330, 2 - 250, 3 - 200. The inset shows the temperature dependence of the forward current at constant voltage.

The capacitance of the investigated heterojunctions depends on the frequency f at which the measurements are carried out (Fig. 1). As follows from the figure, the slope of the straight lines increases with increasing f, and the cutoff voltage V_δ decreases at first, and then at f ≳

1 MHz becomes constant and equal to 1.1 V. The capacitive dispersion is related to the presence of deep recombination centers in the region close to the heterostructure, which are in a charged state. In this case, according to [15], the capacitive cutoff voltage V_δ, will be less than the current V_f, namely

$$V_\delta = V_f - \frac{Q_\delta^2}{2e\varepsilon_0(\varepsilon_1 N_a + \varepsilon_2 N_d)}, \quad (1)$$

where Q_δ is the charge density at the surface levels, N_d and N_a are the concentrations of donors and acceptors, ε_1 and ε_2 are the dielectric permittivities of the heterojunction components, ε_0 is the electric constant. Given that $N_a \ll N_d$ from (1) for Q_δ we obtain the value $4\cdot10^{-8}$ Cl/sм^2, whence $N_s \simeq 3\cdot10^{11}$ sm^{-2}. Note that the calculated minimum value of N_s of the CdS-CdTe heterostructure arising from lattice mismatch is $5\cdot10^{14}$ sm^{-2}, which is 3 orders of magnitude larger than the N_s values determined from experiment according to relation (1).

Considering that the heterojunction capacitance ceases to depend on frequency at f $\gtrsim$ 1 MHz, we can find the recharging time of the levels $\tau = 1/f \simeq 10^{-6}$ s.

Thus, the technology used allows us to obtain HS with a small number of defects at the interface even for semiconductors with very different structures, lattice constants, and thermal expansion coefficients. Such a small N_s has practically no effect on the photosensitivity of the studied structures, but significantly affects the mechanisms of current flow.

The initial parts of the direct branch of the voltampere characteristic of these heterojunctions are satisfactorily described by Newman's empirical formula [1]

$$I = I_{T0}\exp(T/T_0)\exp(V/V_0) \quad (2)$$

where T_0 and V_0 are constants. Usually, to explain such characteristics (Fig. 2), various models of carrier tunneling are involved, which determine the specific type of the I_{T0} multiplier [16]. One of such models is based on the assumption of single- or multistage tunneling through the barrier involving levels at the interface. However, a number of experimental results contradict this model. In particular, the photoconversion efficiency of such diodes reaches 0.8 el/kv, which is once again in favor of sufficient perfection of the interface and low concentration of N_s. In addition, the slope of the straight lines in Fig. 2 slightly increases with decreasing T. The totality of the above facts is well explained in the framework of the tunneling model of thermally excited carriers. In this case, the forward current depends on temperature as $\lg I \sim T^{-1/3}$, which is well fulfilled for the investigated heterojunctions (see the inset in Fig. 2). It should be noted that the tunneling probability of holes is small due to their large mass efficiency as well as the wide bulk charge layer on the CdTe side. Thus, the direct current through the A-type heterojunction is due to the tunneling of electrons from the conduction band of CdS to local states in the forbidden band of CdTe with subsequent recombination. As d_0 decreases (small times and low annealing temperatures), the probability of hole tunneling increases, and the current is tunneling-recombination. The slope of the straight WAC is practically independent of T, which agrees with the theory.

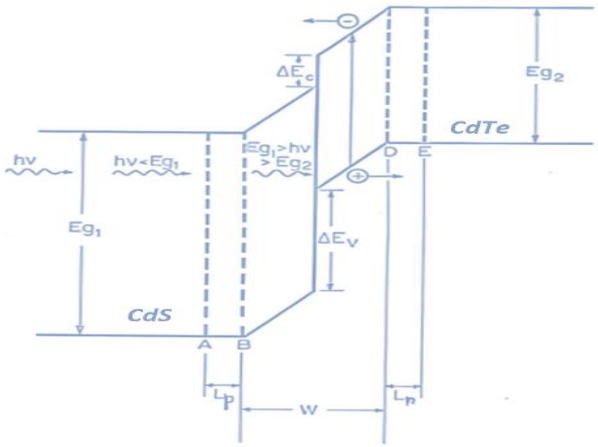

Fig. 3. Band diagram of the CdS-CdTe heterostructure. L_n is the electron diffusion length in the CdTe material, L_p is the hole diffusion length in the CdS material, W is the depletion region width, ΔE_C and ΔE_V are the conduction and valence band discontinuities, E_{g1} and E_{g2} are the band gap width ($E_{g1} > E_{g2}$)

The surface of a wide-bandgap material is illuminated, neglecting for the moment the reflection losses (Fig. 3). Only photons with energy < E_{g1} reach points A, B, C, D and E, and all other photons (with energy -E_{g1}) are absorbed very close to the surface, creating electron-hole pairs. Since they are far from the depletion region, they are not affected by the band bending and hence cannot contribute to the photocurrent. The photons reaching region AB usually have energy < E_{gl}, but there may be very few photons with energy E_{g1} capable of creating electron-hole pairs. If this happens in region AB, the carriers can diffuse into the depletion region, where they are affected by the field and hence contribute to the current. A similar situation occurs in region DE. In region BC, the number of photons reaching this region and capable of creating electron-hole pairs ($h\upsilon > E_{g1}$) is indeed very small, if not zero. Therefore, this region is unlikely to contribute to the current. In the CD region, most, if not all, photons with energies greater than or equal to E_{g2} but less than E_{g1} are absorbed. The carriers created are subject to the field, electrons move to the wide-bandgap material (CdS) where they become majority carriers, and holes move to the narrow-bandgap material (CdTe) where they become majority carriers. (Both have infinite lifetimes). These majority carriers are then collected to form the bulk of the photocarrier. Photons with energies less than E_{g2} pass through the cell and are not absorbed.

Of course, as d_0 increases, the tunneling probability for both holes and electrons decreases. As a consequence, at low forward biases, recombination processes in the space charge region (SCR) become dominant (Fig. 3). The direct current in this case is described by the expression

$$I = I_{gr}^{0} \exp\left(eV/2kT\right) \quad (3)$$

The temperature dependence of the cutoff current I^0_{gr} (at V=0) in the coordinates In I^0_{gr} on $10^3/T$ is approximated by a straight line (see inset in Fig. 4). The activation energy determined from its slope is equal to (1.7 +0.1) eV, which corresponds to the forbidden zone width of the $CdS_x Te_{1-x}$ solid solution at x = 0.6 to 0.7.

At large forward biases, the current for both types of structures (A and B) is thermionic in nature. In this case, the current is mainly electronic, since the barrier height on the CdS side is significantly lower than on the CdTe side. The reverse current of the studied HSs is determined by tunneling of electrons from CdTe to CdS, including through impurity levels.

At large barrier thickness ($d_0 \gtrsim 1$ μm), the processes of current limitation by space charge (CLC) begin to play a significant role. The direct SAW of such heterojunctions is described by the expression

$$I \sim V^m \quad (4)$$

As follows from Fig. 4, it is possible to distinguish up to three sections with different exponent of degree m on I (V) dependences. At the smallest displacements up to a certain voltage V_x m=1, i.e. Ohm's law is satisfied. At $V > V_x$ this dependence changes to a quadratic one, and at $V > V_{fft}$ (full filling of traps) m=8 to10.

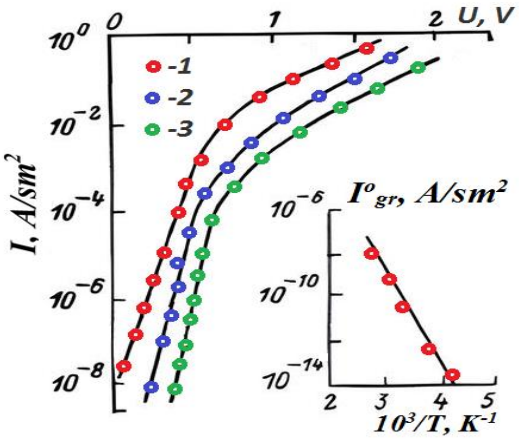

Fig. 4. Straight branches of B-type heterojunction volt-ampere characteristic at different temperatures. T, K: 1 - 360, 2 - 300, 3 - 240. Inset shows the temperature dependence of the cutoff I^0_{gr}

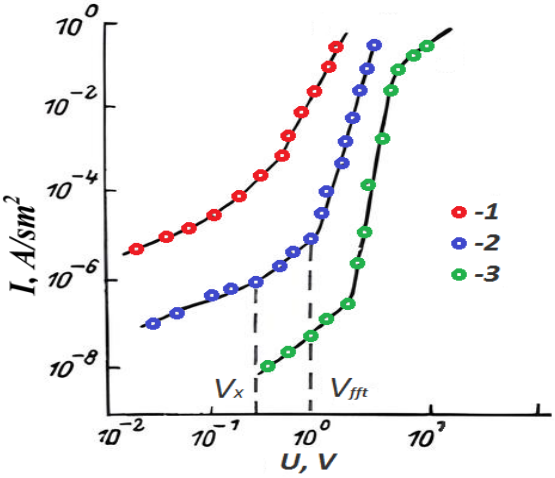

Fig. 5. Straight branches of B-type heterojunction volt-ampere characteristic at different temperatures. T, K: 1 - 340, 2 -230, 3 - 130.

By comparing the experimental data with the theoretical expressions given in, we can determine some parameters of the quasi-isolating layer: carrier concentration n0 and level position.

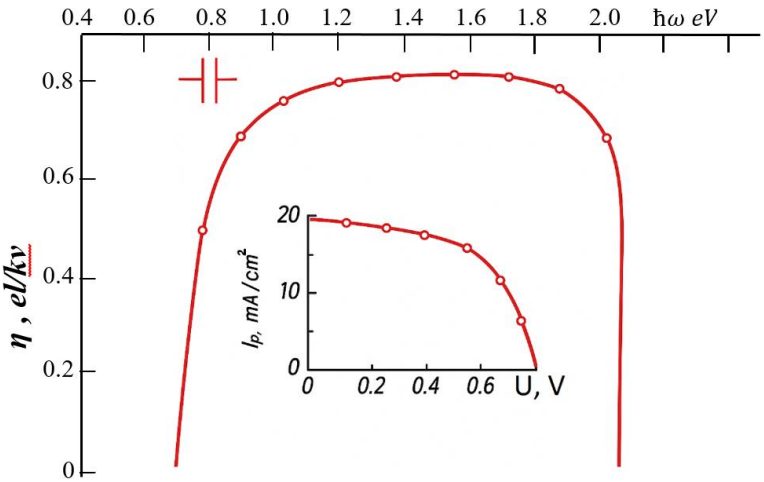

Fig. 6. Photosensitivity spectrum of CdTe-CdS heterojunction at 300 K. Inset shows the load response under AM2 illumination conditions (P= 60 mW/sm^2).

Fermi Fo, the concentration of N, and the depth of occurrence E, of traps. The results of such calculations for one of HS at 300 K are given in the table 1.

Table 1. Calculation results for one of the heterostructures at 300 K

U_x , V	U_{fft}, B	$d_{0,}$ sм	$n_{0,}$ sм$^{-3}$	$F_{0,}$ eV	N_t , sм$^{-3}$	E_t , eV
0.25	0.52	$2\cdot10^{-4}$	10^8	0.60	$2\cdot10^{14}$	0.55

Thus, the direct current of the structures with $d_0 \gtrsim 1$ μm is determined by the injection of electrons from the conduction band of CdS into the high resistivity layer of CdS_x Te_{1-x} solid solutions with subsequent current limitation by space charge.

The studied heterojunctions possessed photosensitivity, and the shape of the spectrum is practically the same for all types of diodes (Fig. 6). The low-energy edge of the spectrum is determined by the generation of photocarriers in the layer with the smallest bandgap width, i.e., ~1.3 eV. The sharp decline of photosensitivity in the region of photon energies $\hbar\omega \gtrsim 2.4$ eV is due to their absorption in the thickness of the CdS crystal. With decreasing temperature, the spectral characteristics shift to the short-wavelength region, and the shape of the spectrum in the investigated temperature range of 100 to 360 K remains practically unchanged. The value of the temperature shift of the long-wavelength and short-wavelength edges of the spectral dependence is equal to $4.4\cdot10^{-4}$ and $5.2\cdot10^{-4}$ eV/K, which is close to the temperature coefficients of the change in the forbidden band width of $CdS_{0.2}$ $Te_{0.8}$ and CdS solution.

As can be seen from Figure 5 the photosensitivity spectra are shifted to the long wavelength region of the spectrum and this indicates that there are deep levels in CdTe responsible for impurity photoconductivity. By analyzing the absorption spectra the deep levels of activation energy are determined, which are equal as shown in Figure 6.

Studies have shown that in all heterojunction short-circuit photocurrent I_{sc} and diode mode photocurrent depend linearly on illumination in a wide range of its variation. With increasing incident light intensity, the no-load voltage V_{id} tends to saturation. At the same time, the absolute values of I_{sc} and V_{id} essentially depend on the type of structure. They are maximal for heterojunction and are 20 mA/sm^2 and 0.6 V under AM2 conditions (see inset in Fig. 5). The decrease in V_{id} in the samples is due to the increase in the dark cutoff current I_{t0} compared to I^0_{gr}. Increasing the thickness of the high resistivity varison layer (type B)

leads to an increase in the series resistance limiting I_{sc}. The efficiency of all types of structures is approximately the same and without the use of enlightening coatings is 0.7 to 0.8 el/kv, which confirms the perfection of the interface and the weak influence of defects on photovoltaic properties.

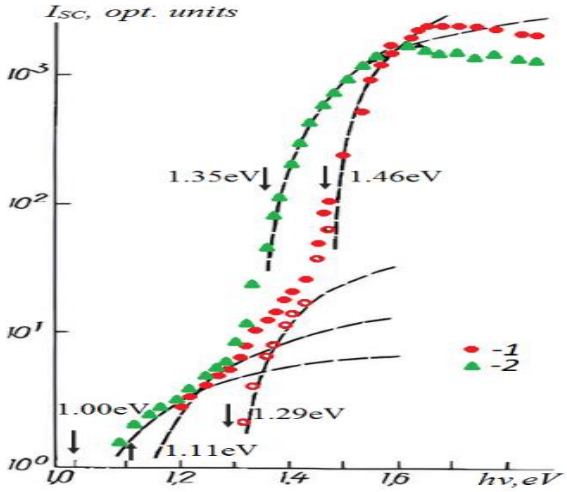

Fig. 7. I_{sc} spectra for CdTe-CdS heterostructure, under frontal illumination. Experimental points: 1- T = 100 K; 2 - T = 300 K. Dotted line - theory.

Fig. 7 shows the spectral dependence of the short-circuit current on the light energy at different temperatures. According to the spectra, the activation energies of deep impurity levels located below the conduction band are definitely 1.00 ± 0.03; 1.35 ± 0.03 and 1.17 ± 0.03; 1.29 ± 0.03 eV, respectively. Hence, the thermal generation of charge carriers also increases with increasing temperature and consequently the effect of additional illumination on the Ikz spectra decreases. For the CdTe-CdS heterostructure, the dominant level is 1.35 ± 0.03, which suggests that this level is associated with silver or its complex with other point defects.

4 Conclusions

Thus, based on the above, it can be said that high photosensitivity in combination with a wide range of linearity and relatively high speed (less than 1 mks at R_U = 100 Ohm) allows using the studied heterostructure as photodetectors in the spectral range of 0.4 to 3.0 eV due to the presence of deep impurity levels. By adding silver impurities, the signal and current power increases. The created heterostructures with a low density of surface states N=3·10^{11}sm^{-2} allow creating high-speed photodetectors in the near infrared region of the spectrum. And as solar cells, it allows accumulating charges in wide ranges of solar radiation up to 0.4 eV to 3.0 eV and have an efficiency of up to 22%.

References

1. N. Sultonov, A.T. Akobirova, R.B. Khamrokulov, O.V. Gafurov, B. Rakhmatov, U.R. Naimov, Electrical properties of cadmium telluride films and a Schottky barrier based on it (Al/CdTe). Bull. Altai State Univ. 4, 2022. URL: https://cyberleninka.ru/article/n/elektricheskie-svoystva-plenok-tellurida-kadmiya-i-bariera-shottki-na-ego-osnove-al-sdte

2. M.A. Scarpulla, B. McCandless, A.B. Phillips, Y. Yan, M.J. Heben, C. Wolden, S.M. Hayes et al., CdTe-based thin film photovoltaics: Recent advances, current challenges and future prospects. Sol. Energy Mater. Sol. Cells 255, 112289 (2023). https://doi.org/10.1016/j.solmat.2023.112289
3. D. Pokhrel, E. Bastola, K.K. Subedi, S. Rijal, M.K. Jamarkattel, R.A. Awni, R.J. Ellingson et al., Copper iodide nanoparticles as a hole transport layer to CdTe photovoltaics: 5.5% efficient back-illuminated bifacial CdTe solar cells. Sol. Energy Mater. Sol. Cells 235, 111451 (2022). https://doi.org/10.1016/j.solmat.2021.111451
4. A.B. Phillips, K.K. Subedi, G.K. Liyanage, F.K. Alfadhili, R.J. Ellingson, M.J. Heben, Understanding and advancing bifacial thin film solar cells. ACS Appl. Energy Mater. 3, 6072–6078 (2020). https://doi.org/10.1021/acsaem.0c00851
5. A. Kumar, S.S. Parida, P. Kumari, D. Chhibber, R. Rai, A.K. Singh, B. Singh, Impedance spectroscopic study of temperature and frequency dependent conduction behaviour of $xBa(Zr_{0.2}Ti_{0.8})O_3–(1-x)(Ba_{0.7}Ca_{0.3})TiO_3$ ceramics. Ceram. Int. 50, 1263–1274 (2024). https://doi.org/10.1016/j.ceramint.2023.10.220
6. Z. Zhang, Y. Liu, Q. Xiong, Accelerating nonadiabatic molecular dynamics simulations in $CdSeXTe_{1}−x$ solar cells with recurrent neural networks. J. Chem. Phys. 163, 024126 (2025). https://doi.org/10.1063/5.0275296
7. E. Artegiani, A. Gasparotto, M. Meneghini, G. Meneghesso, A. Romeo, How the selenium distribution in CdTe affects the carrier properties of CdSeTe/CdTe solar cells. Sol. Energy 260, 11 (2023). https://doi.org/10.1016/j.solener.2023.05.058
8. Q. Sun, Y. Yin, Theoretical exploration of band gap error dependency on band gap size in density functional theory calculations: CdTe and GeTe as representative cases of two band structure semiconductor types. Comput. Mater. Sci. 239, 112956 (2024). https://doi.org/10.1016/j.commatsci.2024.112956
9. W. Solarska, M. Grymuza, M. Kubisa, K. Ryczko, P. Pfeffer, K.P. Korona, K. Karpierz, D. Yavorskiy, Z. Adamus et al., Experiment and k·p analysis of the luminescence from modulation-doped CdTe/(Cd,Mg)Te quantum wells in magnetic fields. Phys. Rev. B 112, 045413 (2025). https://doi.org/10.1103/57md-14wx
10. Y. Zhang, H. Jiang, Z. Yang, L. Fan, Z. Zhang, C. Zhou, Y. Wang, C. Zheng, X. Zhou, P. Chen, Effects of defects in graphene on molecular beam epitaxy of CdTe on graphene/Ge. Appl. Phys. Lett. 127, 011904 (2025). https://doi.org/10.1063/5.0281027
11. T. Sinha, D. Lilhare, A. Khare, A review on the improvement in performance of CdTe/CdS thin-film solar cells through optimization of structural parameters. J. Mater. Sci. 54, 12189–12205 (2019). https://doi.org/10.1007/s10853-019-03651-0
12. I. Jena, P. Singh, U. Unveiling the complex interplay between CdTe film thickness and $CdCl_2$ treatment of CdTe films for solar cell device. J. Mater. Sci.: Mater. Electron. 36, 132 (2025). https://doi.org/10.1007/s10854-025-14211-5
13. K. Iniewski, Semiconductor materials for direct conversion: Si, CdTe, and CdZnTe. In: *Direct Conversion Semiconductor Radiation Detectors using Si, CdTe and CdZnTe*. Springer, Cham (2025 https://doi.org/10.1007/978-3-031-94005-7_2
14. Z. KordGhasemi, H. Eshghi, Enhanced photoresponse in Ag/CdTe/p-Si/Al heterostructure photodetectors: The influence of CdTe layer thickness. J. Mater. Sci.: Mater. Electron. 35, 739 (2024). https://doi.org/10.1007/s10854-024-12515-6
15. S. Tyagi, U.R. Meena, S. Kumar et al., Effect of lattice mismatch on orientation of MBE grown CdTe on GaAs(211). J. Mater. Sci.: Mater. Electron. 36, 944 (2025). https://doi.org/10.1007/s10854-025-15033-1
16. S.J. Martin, A.B. Walker, A.J. Campbell, D.D.C. Bradley, Electrical transport characteristics of single-layer organic devices from theory and experiment. J. Appl. Phys. 98, 063709 (2005). https://doi.org/10.1063/1.2058199